Carrier Frequency Recovery in All-Digital Modems for Burst-Mode Transmissions

Marco Luise, *Member, IEEE*, and Ruggero Reggiannini

Abstract—**Reliable data detection in Time Division Multiple Access (TDMA) communication systems strictly depends on the availability of accurate estimates of the synchronization parameters of the received signal, i. e., carrier frequency/phase and symbol timing, which must be derived from the burst preamble. In this paper we focus on the carrier frequency estimation aspect, and we present a fast, open-loop, all-digital frequency offset estimation technique, whose performance is assessed in two different communication scenarios: a TDMA satellite link employing standard modulation and burst formats, and a mobile cellular terrestrial radio system with signal and channel characteristics obeying the pan-European Group Spècial Mobile (GSM) recommendations. The use of the algorithm as a frequency error detector (discriminator) in a recursive ("closed-loop") frequency offset estimator is also discussed, and some results concerning both the transient and the steady-state behavior of such a scheme are presented. Finally, the impact of the algorithm on the receiver BER is briefly analyzed.**

I. Introduction

Time division multiple access techniques, although primarily developed for satellite links [1], have grown popular in a variety of application areas, notably in terrestrial mobile cellular systems and wireless communications [2]. As is known, each TDMA data burst includes a sequence of training bits (preamble) which are exploited by the receiver for burst identification as well as for carrier and symbol timing recovery.

Focusing on the carrier frequency recovery problem, a number of fast-converging methods for its solution have been presented in the literature, most of which are intended for application with linearly modulated, burst-mode signals transmitted over the Additive White Gaussian Noise (AWGN) channel. Among these techniques, we mention the maximum-likelihood (ML) method for PSK signals proposed in [3], whereby a periodic sequence of training bits is recursively passed through a bank of bandpass filters (implemented in the form of a discrete Fourier transform) whose frequency spacing is varied so as to achieve an accurate estimate of the frequency at which the input signal spectrum peaks. An alternative scheme proposed in [4] employs a sort of differential detector whose output is sampled at symbol rate and appropriately processed to remove modulation, so as to obtain a complex-valued sequence of samples whose phase depends on the carrier frequency offset and not on data symbols. Paper [5] presents an algorithm for carrier synchronization which does not require the presence of the training symbol sequence. As in the previous case, differential symbol estimates are used to cancel data modulation from the received signal, thus obtaining a sequence of samples whose average phase slope is proportional to the frequency offset. As a next step, the cited phase slope is evaluated by means of a fitting technique analogous to that illustrated in [6]. A similar approach was also developed and analyzed in [7].

The problem of carrier frequency recovery may be sometimes circumvented by imposing stringent requirements on the frequency stability of the transmit and receive oscillators. For instance, GSM recommendations [8] demand that the uncompensated frequency offset at the demodulator output should not exceed a few hundred Hz inclusive of Doppler shifts, thus calling for oscillator stabilities better than 10^{-7}. This seems a rather severe constraint, and some methods for its relief would be of interest.

In this paper, we present an efficient technique for fast carrier frequency offset recovery based on data modulation and/or channel distortion removal from the received signal. As was done in [9] by Fitz, our algorithm was derived from ML estimation theory, and its error performance in the absence of fading was observed to lie very close to the Cramér-Rao lower bound (CRLB) for unbiased estimators [10], [11]. We also present a simple implementation of the algorithm, which is made up of a few standard digital signal processing (DSP) components (Section II). As a next step, the algorithm is applied to two different communication scenarios: a typical TDMA satellite link and a mobile cellular terrestrial radio system with signal and channel characteristics obeying the pan-European GSM recommendations [12] (Section III). We also show how the scheme can operate as a frequency error detector within a closed loop tracker (Section IV). A summary and some final remarks conclude the paper (Section V).

II. Frequency Offset Estimation

A. Frequency estimation algorithm

We consider the problem of ML estimation of the frequency Δf of the complex-valued oscillation $\exp\{j2\pi\Delta ft\}$, starting from the observation of the sampled signal

$$r_k = e^{j(2\pi\Delta fkT_s+\theta)} + v_k, \quad 1 \le k \le N \tag{1}$$

Paper approved by Marc Moeneclaey, the Editor for Synchronization of the IEEE Communications Society. Manuscript received September 29, 1992; revised May 10, 1993. The work was carried out in the framework of the Research Program "Prometheus/PRO-COM" funded by the European Union. This paper was presented in part at the 3rd Int. Workshop on DSP Techniques Applied to Space Communications, ESA/ESTEC, Noordwijk (The Netherlands), September 1992, and at the IEEE Communication Theory Mini-Conference CTMC '92, Orlando FL, December 1992.

The authors are with the University of Pisa, Dipartimento di Ingegneria dell'Informazione, Via Diotisalvi 2, 56126 Pisa, Italy.

IEEE Log Number 9410912.

where $T_s \le 1/(2\Delta f)$ is the sampling interval, θ is an unknown random phase with uniform probability density in $[0, 2\pi)$ and $v_k = v_{k,c} + jv_{k,s}$, $\{v_{k,c}\}$ and $\{v_{k,s}\}$ being independent zero-mean Gaussian random sequences, both with autocorrelation $R_v(k) = \sigma^2 \delta_{k,0}$ ($\delta_{k,j}$ represents here the Kronecker's symbol). This problem is well developed in the literature [14], [15], so that, skipping all details for brevity's sake, we are led to the problem of seeking the maximum of the equivalent likelihood function

$$\Lambda(\Delta\tilde{f}) \triangleq \left| \sum_{i=1}^{N} r_i e^{-j2\pi \Delta\tilde{f} i T_s} \right|^2 = \sum_{k=1}^{N} \sum_{m=1}^{N} r_k r_m^* e^{-j2\pi \Delta\tilde{f} T_s (k-m)} \tag{2}$$

where $\Delta\tilde{f}$ is a tentative value for Δf. Maximizing (2) with respect to $\Delta\tilde{f}$ yields the ML estimate of Δf, $\Delta\hat{f}_{ML}$, which is consistent and also asymptotically efficient [10] insofar as for $N \to \infty$ its variance equals the so-called Cramér-Rao Lower Bound (CRLB) σ^2_{CR}, a fundamental (i. e., that cannot be surpassed by any estimator) lower limit to the variance of any unbiased frequency estimator operating on a signal modeled as in (1) [11]. The CRLB for our problem is easily found to be

$$\sigma^2_{CR} = \frac{3}{2\pi^2 T_s^2} \frac{1}{\rho N(N^2-1)} \tag{3}$$

where ρ indicates the carrier-to-noise ratio (CNR), defined as the ratio between the signal and noise powers in (1):

$$\rho \triangleq \frac{1}{2\sigma^2}. \tag{4}$$

Unfortunately, a simple, closed-form solution to the problem of maximizing (2) cannot be derived, so that an exact determination of $\Delta\hat{f}_{ML}$ would require a numerical calculation, which is a complex and time-consuming task. An alternative suboptimal technique, providing estimates close to the CRLB with a moderate computation complexity, is introduced in the following.

Taking the derivative of (2) with respect to $\Delta\tilde{f}$ and equating it to zero yields

$$\sum_{k=1}^{N} \sum_{m=1}^{N} (k-m) r_k r_m^* e^{-j2\pi \Delta\tilde{f} T_s (k-m)} = 0 \tag{5}$$

or, rearranging terms,

$$\mathrm{Im}\left\{ \sum_{k=1}^{N-1} k(N-k) R(k) e^{-j2\pi \Delta\tilde{f} k T_s} \right\} = 0 \tag{6}$$

where $R(k)$ denotes the estimated autocorrelation of the sequence r_k, defined as

$$R(k) \triangleq \frac{1}{N-k} \sum_{i=k+1}^{N} r_i r_{i-k}^*, \quad 0 \le k \le N-1 \tag{7}$$

Equation (6) represents a necessary condition for the solution of our maximization problem to exist. Particular care must be taken in order to avoid those zeroes of (6) corresponding to local maxima of (2) different from the solution of the likelihood equation (the absolute maximum). The "false maxima" can be avoided by appropriately restricting the operating range of the estimator, as will be shown in the sequel. We notice now that the term in braces in (6) can be thought of as the Discrete Fourier Transform of the estimated autocorrelation $R(k)$, weighted by the parabolic windowing function $w(k) = k(N-k)$, $k = 1, 2, \ldots, N-1$. This weighing function accounts for the fact that, in the vicinity of $k = 0$, the autocorrelation $R(k)$ bears intrinsically little or no information on the frequency offset because it is derived from closely spaced signal samples. On the other hand, when k is close to N, $R(k)$ becomes a poor estimate of the autocorrelation of r_k, since the number of terms in the sum (7) building up such an estimate is small. In a suboptimum implementation of the frequency estimator, $w(k)$ can be replaced by a rectangular sequence made up of all 1's, $k = 1, 2, \ldots, M$, $M \le N-1$, to discard the unreliable autocorrelation estimates close to $k = N$, while retaining the "good" autocorrelation samples near $k = 1$. We obtain thus the following modified estimation strategy:

$$\mathrm{Im}\left\{ \sum_{k=1}^{M} R(k) e^{-j2\pi \Delta\tilde{f} k T_s} \right\} = 0. \tag{8}$$

For an ideal noiseless channel, $R(k) = \exp(j2\pi \Delta f k T_s)$ and $\Delta\tilde{f} = \Delta f$ is still a trivial solution of the modified estimation strategy (8). When noise is present, the solutions of (6) and (8) will differ in general but, with a proper choice of M, their mean squared distance is expected to get negligible as the CNR increases.

Under the assumptions of high CNR and low frequency deviation ($M \Delta f T \ll 1$), an approximate way of solving (8) can also be devised. In fact, replacing the exponential in (8) by its Taylor series expansion truncated to the linear term and rearranging, we get

$$\Delta\hat{f} \cong \frac{1}{2\pi T_s} \frac{\sum_{k=1}^{M} \mathrm{Im}\{R(k)\}}{\sum_{k=1}^{M} k\, \mathrm{Re}\{R(k)\}} \tag{9}$$

which immediately yields the estimate $\Delta\hat{f}$. We can also work out a simpler version of (9), which is better oriented to a straightforward DSP implementation of the frequency estimation algorithm, by arguing that under the above assumptions $R(k) = \exp(j2\pi \Delta f k T_s) + \tilde{v}_k \cong 1 + j2\pi k \Delta f T_s + \tilde{v}_k$, with $\tilde{v}_k$ an appropriate noise term, $|\tilde{v}_k| \ll 1$, so that

$$\sum_{k=1}^{M} \mathrm{Im}\{R(k)\} \cong M \arg\left\{ \sum_{k=1}^{M} R(k) \right\} \tag{10}$$

$$\sum_{k=1}^{M} k\, \mathrm{Re}\{R(k)\} \cong \frac{M(M+1)}{2} \tag{11}$$

where $\arg(z)$ denotes the argument of the complex number z, taken in the interval $[-\pi, \pi)$. Collecting (9)-(11), we are finally led to

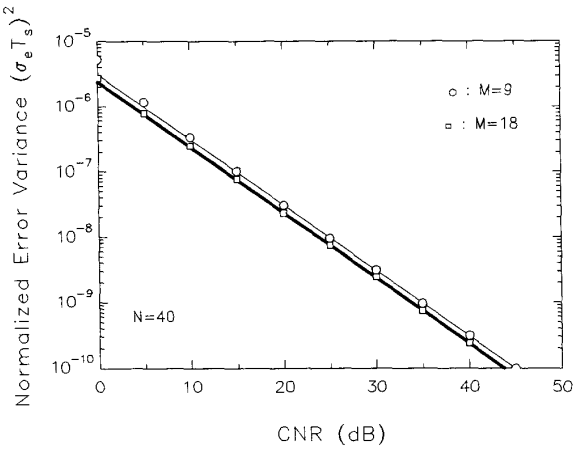

Fig. 1 - Normalized variance of the frequency estimation error for algorithm (12).

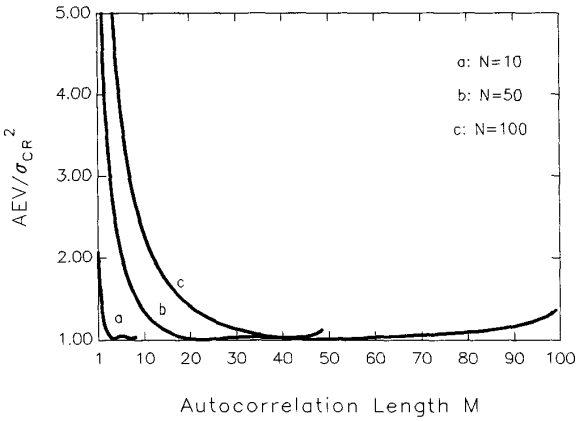

Fig. 2 - Dependence on M of the estimator performance.

$$\Delta\hat{f} \equiv \frac{1}{\pi T_s (M+1)} \arg\left\{\sum_{k=1}^{M} R(k)\right\} \tag{12}$$

which represents the final form of the frequency estimation algorithm we will focus on in the following. We note that $\Delta\hat{f}$ is correctly determined as long as the argument of the summation at the right-hand side of (12) does not exceed $\pm\pi$. This limits the operating range of our frequency recovery scheme to the interval

$$|\Delta f| < [(M+1)T_s]^{-1}. \tag{13}$$

where no ambiguity problems arise (see Eq. (2)). The proposed estimator is a generalization of a similar algorithm analyzed in [16], obtained from (12) by letting $M=1$. As already mentioned, an approximate-ML frequency estimation algorithm similar to (12), but with a somewhat higher implementation complexity, is also discussed in [9]. However, very few performance results about the frequency recovery scheme could be found therein.

B. Algorithm performance

We found that estimator (12) is asymptotically unbiased and we derived an expression of the estimation error variance σ_e^2 when the CNR is large, hereafter referred to as *asymptotic error variance* (AEV) of the algorithm. The calculation of the AEV under the assumption $2\pi\Delta f T_s M \ll 1$ is outlined in the Appendix. The final result is

$$\sigma_e^2\big|_{\rho\to\infty} \triangleq E\{(\Delta\hat{f}-\Delta f)^2\}\big|_{\rho\to\infty} \to \frac{1}{\pi^2 T_s^2 (M+1)^2} \cdot \frac{1}{\rho M^2} \sum_{m=1}^{M}\sum_{r=1}^{M} \left\{ \frac{\min(N-r, N-m)}{(N-r)(M-m)} - \frac{(N-r-m)\mathrm{u}(N-r-m)}{(N-r)(M-m)} \right\} \tag{14}$$

where $\min(\cdot,\cdot)$ indicates the minimum between its two arguments and $\mathrm{u}(\cdot)$ is the unit step function. Figure 1 shows the normalized frequency error variance $(\sigma_e T_s)^2$ plotted as a function of ρ, for $N=40$, $\Delta f = 0$ and two different values of M. Solid thin lines represent the AEV (14), while symbols denote simulation results, obtained with the aid of the tool SPACE (Software PAckage for Communication Engineering) developed at the University of Pisa. Also shown for comparison is the normalized CRLB (thick curve). A remarkably good agreement between analysis and simulation is observed at medium-to-high values of CNR. Although the results in Fig. 1 are obtained for $\Delta f = 0$, as will be apparent in the sequel (see Fig. 6), the error variance $(\sigma_e T_s)^2$ is remarkably independent of the particular value of Δf, as long as the frequency offset stays within the operating range (13). Also, in the CNR range considered in Fig. 1, we did not observe any threshold effect in the estimator variance; this closely resembles the results presented in [14] about the "true" ML estimator of Δf.

It can also be seen that for M exceeding a few units (say, $M \geq 10$), the AEV curves approach closely the CRLB.The effect of a variation of M for a fixed N is illustrated in Fig. 2, where the ratio of the AEV to the CRLB is plotted vs. M, for different values of N. From these curves it is seen that the optimum (i. e., with minimum departure from the CRLB) value of M is approximately $N/2$ when $N \gg 1$. Throughout the following, without further mention, M will be assumed equal to this optimum value.

As previously noted, algorithm (12) yields correct frequency estimates in the frequency offset range given by (13), so that application of the algorithm requires some control on the maximum allowable frequency deviation of the signal.

C. Algorithm implementation

Algorithm (12) can be implemented by means of a few standard DSP components, as illustrated in Fig. 3. This scheme is easily obtained after inserting (7) in (12) and interchanging the summations on k and i. An $N-$tap shift register, which is to be initialized with a sequence of all 0's, is supplied with the complex-conjugated sequence (1). At each clock step, the

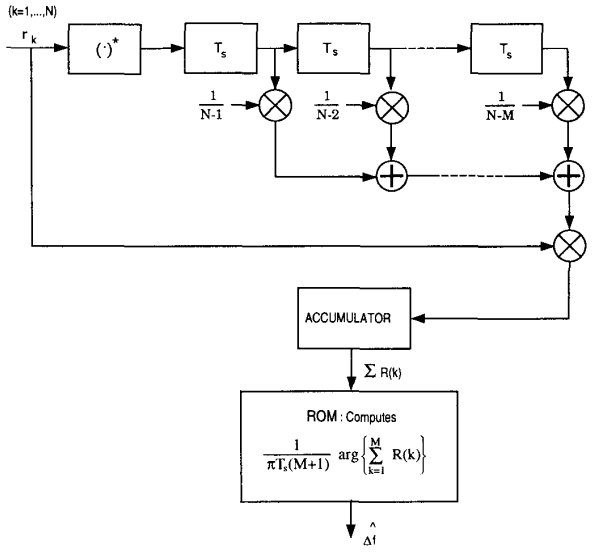

Fig. 3 - Implementation of the estimator by means of DSP components.

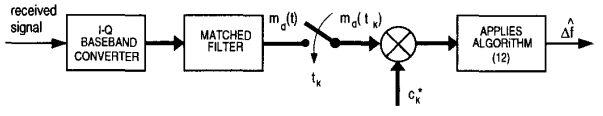

Fig. 4 - Open-loop frequency recovery scheme for the satellite TDMA system. Thick lines indicate complex-valued signals.

contents of the register are shifted, multiplied by the weights $1/(N-i), i=1,2,\ldots,M$, and summed up together. This type of processing is just that encountered in an FIR filter implementation. The output of such a filter is multiplied by the input signal r_k and the result is accumulated so as to build up the summation at the right-hand side of (12), whose argument is then extracted and appropriately scaled by a Read-Only Memory (ROM). It is noted that the FIR filter has a complex-valued input and $M < N$ real taps, so that each of the corresponding multipliers and adders are implemented as two decoupled real-input components, while the final multiplier by r_k is a true complex multiplier made of four real multipliers and two real adders. Evaluation of a frequency estimate according to the scheme of Fig. 3 calls for a total of $2NM+4N$ real products, $2N(M-1)+2N-2$ real additions and a ROM access.

Adopting the optimum value $M = N/2$, it is seen that the computational complexity of the estimator grows as N^2, due to the operation of FIR filtering described above. Thus, for large values of N such a filtering might call for an FFT-based implementation. On the other hand, since M can be substantially reduced with respect to its optimum value $N/2$ (say, by a factor 2 to 3) without losing much of the optimality of the estimator (see Fig. 2), and since in most burst-mode communication applications N is in the order of a few tens, the convenience of an FFT-based filtering might be questioned. As a final remark on this subject, we observe that the linear-regression algorithm presented in [6] has a complexity proportional to N, but reaches the CRLB only for large values of E_b/N_0.

III. Two Applications of the Algorithm

A. Satellite TDMA

Figure 4 shows the application of the previously described frequency estimator to a bandlimited QPSK receiver, suited for satellite TDMA systems. Assuming equally-split Nyquist filtering, the expression of the sampled, frequency-shifted and noise-corrupted preamble signal is

$$m_d(t_k) = m(t_k)\exp[j(2\pi\Delta f t_k + \phi)] + n(t_k), \quad t_k \in (\tau_1, \tau_2) \tag{15}$$

where ϕ is the carrier phase, $t_k \triangleq kT + \tau$ are the sampling instants, $0 \le \tau < T$ denoting a possible timing offset, $m(t_k)$ is the filtered and baud-rate sampled burst preamble, (τ_1, τ_2) is the observation interval and $n(t_k)$ are independent samples of a complex-valued Gaussian process whose real and imaginary components have variance $\sigma_n^2 = N_0/T$. We explicitly observe that the signal model (15) can be considered valid as far as the frequency offset Δf is small (i. e., a few percent) compared to the symbol rate, so that the mismatch of the Nyquist root-raised-cosine receive filter due to the frequency offset can be neglected. This is not a severe constraint in view of the typical operating range of the frequency estimator (Sect. 2.1). Under the assumption of perfect timing recovery ($\tau = 0$), we have $m(t_k) = c_k$, where c_k is the k-th transmitted QPSK symbol, so that

$$m_d(t_k) = c_k\sqrt{2P}\exp[j(2\pi\Delta f t_k + \phi)] + n(t_k), \quad t_k \in (\tau_1, \tau_2) \tag{16}$$

where P is the received average signal power. Dividing (16) by $m(t_k) = \sqrt{2P}c_k$, a complex-valued oscillation plus noise results

$$\frac{m_d(t_k)}{m(t_k)} = m_d(t_k)c_k^*/\sqrt{2P} = \exp[j(2\pi\Delta f t_k + \phi)] + v(t_k), \quad t_k \in (\tau_1, \tau_2) \tag{17}$$

where the noise term is defined as

$$v(t_k) \triangleq \frac{n(t_k)}{m(t_k)} = \frac{n(t_k)c_k^*}{\sqrt{2P}} \tag{18}$$

The complex samples $v(t_k)$ are Gaussian independent with independent I-Q components having a variance $\sigma^2 = N_0/2PT = (4E_b/N_0)^{-1}$, where E_b/N_0 is the energy-per-bit-to-one-sided-noise-spectral-density ratio. The properties of sequence (17) are thus identical to those of sequence (1) and the results derived in Sect. 2.2 for the frequency recovery algorithm apply exactly to the present case provided that T_s and ρ are replaced by T and $2E_b/N_0$, respectively. In addition to those results, Figs. 5 and 6 show the mean and the RMS value of the frequency estimates as a function of the normalized frequency offset ΔfT with perfect timing recovery, derived by simulation

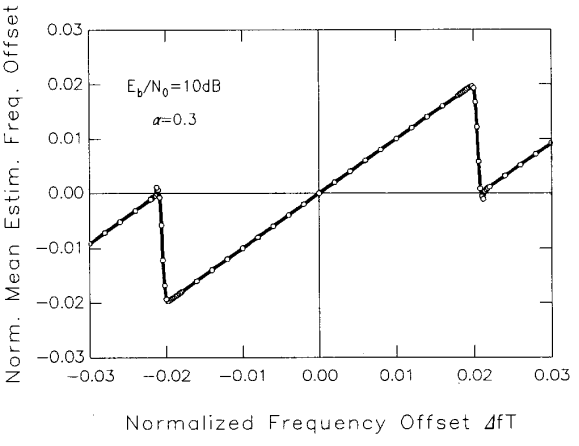

Fig. 5 - Average frequency estimate for the QPSK signal with perfect symbol timing recovery.

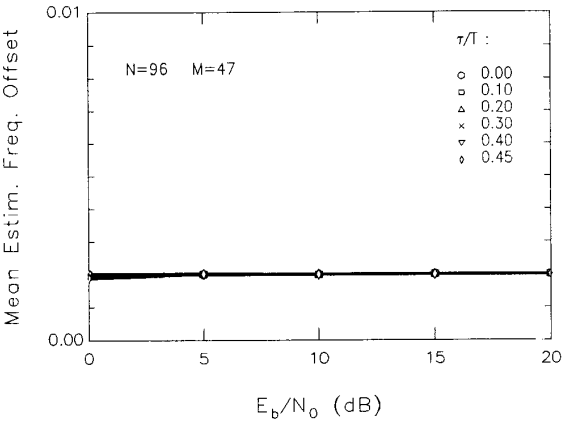

Fig. 7- Average frequency estimate for the QPSK signal with symbol timing error.

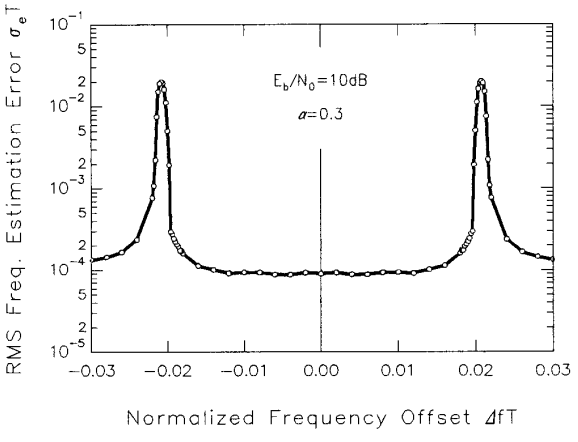

Fig. 6 - RMS frequency estimation error for the QPSK signal with perfect symbol timing recovery.

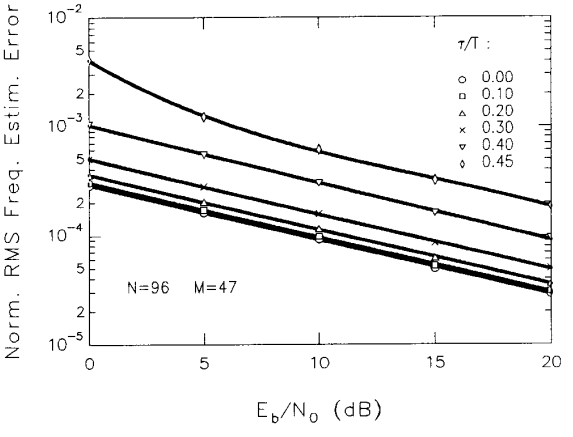

Fig. 8 - RMS frequency estimation error for the QPSK signal with symbol timing error.

for a standard sign-alternating BPSK symbol sequence preamble. The curves were obtained letting E_b/N_0 =10 dB, N=96, M=47 and assuming α=0.3. As expected, the curves of Fig. 5 are linear and cross the Δf axis at the origin and also at the frequencies $\pm[(M+1)T]^{-1}$. The diagrams confirm that the estimates are practically unbiased in a broad range around $\Delta f = 0$, and reveal that the error variance is almost flat in the same region. When Δf approaches the limit-values $\pm[(M+1)T]^{-1}$, the estimator exhibits an increasing bias due to the discontinuity of the arg{·} function in (12), so that the RMS estimation error grows considerably.

In the previous analysis, we assumed that symbol timing is known at the receiver (i. e., $\tau = 0$). This assumption seems reasonable in view of the high stability of timing references used in TDMA systems, and also considering that the timing estimates can be periodically updated by means of clock extraction algorithms [18] providing correct operation in the range of frequency offsets typical of our application. Nonetheless, Figs. 7-8 show the effect of a non-negligible timing error τ on the curves of the statistical expectation and RMS value of the estimates as a function of E_b/N_0, with $\Delta f = 2\cdot 10^{-3}/T$. It is seen that the presence of a nonzero sampling offset does not introduce any further estimation bias, whereas the error variance of the estimator may undergo a substantial degradation, due to the presence of intersymbol interference.

B. GSM transmissions.

As is known, in the pan-European digital cellular mobile radio communication system GSM, the recommended modulation format is Gaussian Minimum Shift Keying (GMSK) with a normalized bandwidth factor βT_b=0.3 [12], where $1/T_b$ =270.8 kb/s is the channel bit rate. A nice property of the GMSK signal is its close similarity to an Offset

Quadrature Phase-Shift Keying (OQPSK) signal with an appropriate elementary pulse shape $g(t)$ [13]. Accordingly, GMSK can be regarded as an approximately linear offset modulation, so that the complex envelope of the N_b-bit long received burst (N_b=148) can be expressed as follows:

$$s(t) \cong \sum_{k=0}^{N_b/2-1} a_k h(t-2kT_b) + j \sum_{k=0}^{N_b/2-1} b_k h(t-2kT_b-T_b) \quad (19)$$

where a_k and b_k are IID symbols drawn from the alphabet $\mathcal{A}=\{-1,1\}$, $h(t)$ is the overall transmitter-plus-channel impulse response, i. e., $h(t) \triangleq g(t) \otimes c(t)$, $c(t)$ being the impulse response of a Rayleigh-fading multipath propagation channel as described in [18]. The delays and attenuation profiles for the typical urban (TU), rural area (RA) and hilly terrain (HT) channels can be found in [18] as well. As is customary, the function $h(t)$ will be denoted in the sequel by the acronym CIR (Channel Impulse Response), not to be confused with $c(t)$.

According to the GSM specifications, the known 26-bit training sequence is allocated in the central portion of the burst, and is thus also called *midamble*. We can extract the midamble from the rest of the burst and write it in a form similar to (19):

$$m(t) \triangleq m_R(t) + jm_I(t)$$
$$= \sum_{k=0}^{N_m-1} \alpha_k h(t-2kT_b) + j \sum_{k=0}^{N_m-1} \beta_k h(t-2kT_b-T_b) \quad (20)$$

where the time origin has been properly shifted and $\{\alpha_k\},\{\beta_k\}$ denote the I and Q training sequences, of length N_m=13 bits. It is noted that symbols coming before and after the midamble may introduce a non negligible level of ISI at the boundaries of $m(t)$, that is not accounted for in (20).

In the all-digital GSM demodulator [12], the received signal is frequency-shifted, passed through a low-pass channel filter (an 8-pole Butterworth filter with bandwidth $0.375/T_b$) and digitized at the rate $1/T_c$. The noise-corrupted midamble portion of the burst can thus be written in a form akin to (15):

$$m_d(t_k) = m(t_k)\exp[j(2\pi\Delta f t_k + \phi)] + n(t_k), \quad t_k \in (\tau_1, \tau_2) \quad (21)$$

where $t_k \triangleq kT_c + \tau$, T_c and $\tau \in [0, T_c]$ being the sample spacing and delay, respectively, $m(t)$ is the received midamble, ϕ is a constant phase and (τ_1, τ_2) is the observation interval. The channel filter is no longer matched to the incoming signal, and its bandwidth is supposed wide enough to let the useful signal pass undistorted, while bandlimiting the noise $n(t)$.

If we could exactly estimate the CIR $h(t)$ from observations (21), we could also generate a distortion-free replica of the midamble $m(t_k)$ within the receiver. Then, dividing (21) by $m(t_k)$, a complex oscillation plus noise similar to that at the right-hand side of (17) would result. Unfortunately, the actual CIR estimate (as obtained for instance through the standard procedure outlined in [12]) is somewhat distorted even with a non-dispersive channel as an effect of thermal noise and of the uncompensated frequency offset in (21), so that a performance degradation with respect to the ideal (as well as to the preceding TDMA) case is to be expected.

Let now $m_r(t_k)$ denote the locally remodulated midamble in the interval $t_k \in (\tau_1', \tau_2')$, i. e., in a convenient subset of (τ_1, τ_2) where the boundary interference effects can be disregarded ($\tau_2' - \tau_1' = 20T_b$, corresponding to $N = 21$ in the algorithm (7)-(12)). Then, dividing (21) by $m_r(t_k)$ yields the sequence

$$p(t_k) = q(t_k)\exp[j(2\pi\Delta f t_k + \phi)] + v(t_k), \; t_k \in (\tau_1', \tau_2') \quad (22)$$

where

$$q(t_k) \triangleq \frac{m(t_k)}{m_r(t_k)}, \; v(t_k) \triangleq \frac{n(t_k)}{m_r(t_k)} \quad (23)$$

For moderate distortion, $q(t_k)$ keeps close to unity, and $p(t_k)$ can be considered a good approximation of the sequence (1) provided that the noise samples $v(t_k)$ are Gaussian independent. This condition is exactly met when the sampling interval T_c equals or exceeds the correlation time of the process $n(t)$, i. e., approximately the inverse of the channel filter bandwidth, or, in the GSM receiver, $\sim 1.33T_b$ [12]. However, for ease of implementation, in all of our evaluations we found it convenient to sample the signal at bit rate.

Figures 9-10 show plots of the mean value of $\Delta\hat{f}$ as a function of Δf for different values of E_b/N_0 when the propagation channel is stationary, with $c(t) = \delta(t)$ (ideal stationary (IS) channel). As is seen from Fig. 9, the curves are now nonlinear and intersect the Δf axis close to the origin and at two further points placed asymmetrically around $\Delta f = 0$, approximately at f_1=-13.5 kHz and f_2=10.5 kHz. Thus the frequency estimates exhibit a bias that grows with $|\Delta f|$ and with the inverse of E_b/N_0. This undesirable behavior is the result of the CIR estimation errors due to the presence of channel Gaussian noise and, to a lesser extent, of ISI inherent to the GMSK signal. Errors in CIR estimation due to the asymmetric spectral properties of the GSM channel probe sequence (20) are also responsible for the asymmetry of the average estimated frequency with respect to Δf exhibited by the curves in Fig. 9. Finally, Fig. 11 shows the standard deviation σ_e of the frequency estimation error as a function of Δf and E_b/N_0 in the same frequency range as in Fig. 9.

IV. Frequency Tracking Loop

The accuracy attained by a single-burst estimation was illustrated in Figs. 5-8 for the satellite link and in Figs. 9-11 for the GSM system with an IS channel. Although this performance can be considered excellent in itself, as it closely approaches the CRLB, the residual frequency fluctuations after baseband conversion may still be too large, thus causing excessive phase rotations in the burst data section. Therefore, if the frequency sources in the system are stable over a sequence of consecutive bursts (as happens when the carrier frequencies, either fixed or frequency-hopped, are generated by means of a synthesizer driven by a single stable oscillator, and the Doppler shift rate is negligible), then the algorithm accuracy can be trivially improved by averaging a number L of consecutive single-burst estimates. For the GSM system, for instance, an RMS asymptotic error allowing correct receiver

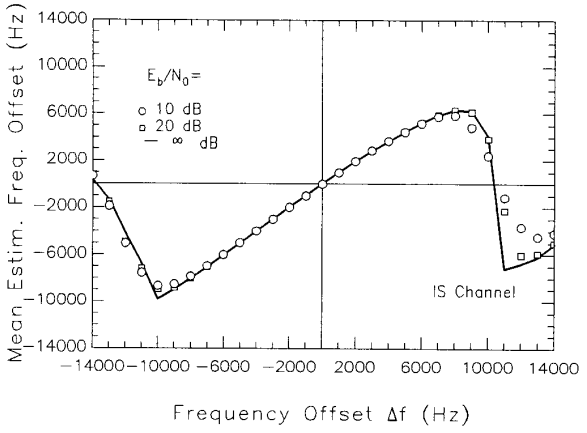

Fig. 9 - Average frequency estimate for the GSM system. Perfect symbol timing recovery.

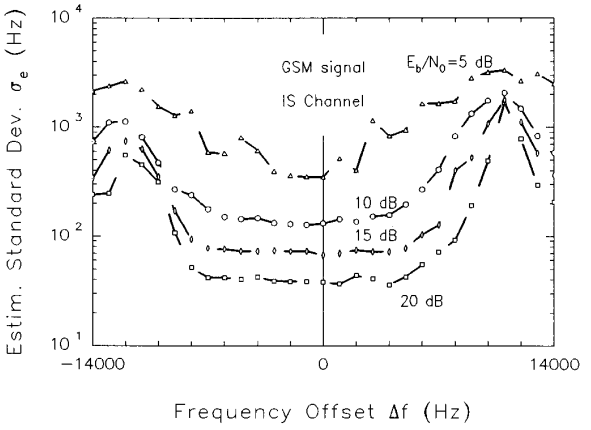

Fig. 11 - RMS frequency estimation error for the GSM system. Ideal channel conditions.

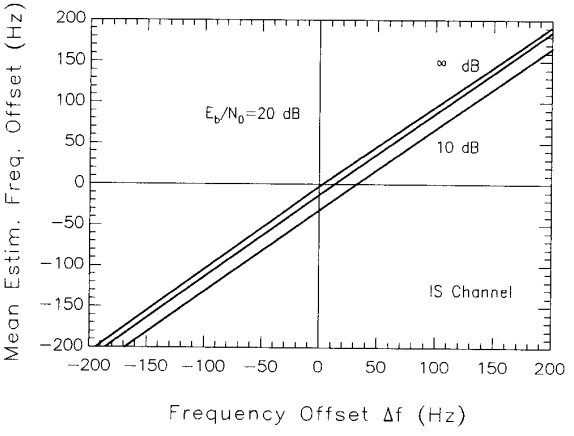

Fig. 10 - Close-up of Fig. 9 in the vicinity of Δf=0.

operation can be attained by averaging as few as $L = 10 \div 20$ estimates for E_b/N_0 ranging from 5 dB to 10 dB on the ideal channel. This technique can be implemented directly in an open loop configuration similar to that shown in Fig. 4 so as to provide frequency estimates from the observation of (nonoverlapping) groups of L consecutive bursts, with every estimate used to correct the frequency offset in the subsequent L bursts. This scheme is simple to implement and is unconditionally stable but, as pointed out in Sect. 3.2, it may suffer, in the case of the GSM receiver, from the presence of an error bias induced both by thermal noise and imperfect knowledge of the signaling pulse shape.

The cited drawback may be overcome by a recursive ("closed loop") scheme, wherein the frequency estimate at step k is used to *correct*, and not to replace, the one available at step $k-1$, until the estimation error is brought down to negligible levels. Figure 12 shows the functional block diagram of a receiver utilizing such a mixed open-loop/closed-loop frequency tracker. The received signal, after baseband conversion, is passed through an antialiasing stage, then sampled at the rate $f_c = 1/T_c$, A/D converted and frequency downshifted by the amount $\delta\hat{f}_k$, i. e., by the closed-loop frequency estimate at step k. This estimate is related to $\delta\hat{f}_{k-1}$ as follows

$$\delta\hat{f}_k = \delta\hat{f}_{k-1} - \gamma\Delta\hat{f}_{k-1}\,, \tag{24}$$

where γ is the updating stepsize and $\Delta\hat{f}_{k-1}$ is now the estimate of the *residual* frequency offset $f_{\Delta,k-1}$ at step $k-1$, $f_{\Delta,k-1} \triangleq \Delta f - \delta\hat{f}_{k-1}$, derived according to (12) from observation of L consecutive bursts at the output of the matched (or channel) filter. Three different operating rates may now be identified in the scheme of Fig. 12: $1/T_c$ in the digital front-end filtering, $1/T$ for TDMA or $1/T_b$ for GSM after filtering, for data estimations (decimator not shown), and the frequency estimate update rate $1/T_\Delta$, $T_\Delta \triangleq T_{FRAME} \cdot L \gg T_c$, where T_{FRAME} is the frame repetition period.

The tracking performance of algorithm (24) can be analyzed through standard techniques under the assumption that the tracking error is small enough to allow for loop linearization [19]. The performance of the system depicted in Fig. 12 was evaluated in the most challenging of the two scenarios outlined in the previous section, namely, GSM mobile transmissions. Theoretical analysis was focused on the evaluation of the tracking error jitter variance, while simulation was used to assess both the steady-state and the transient behavior of the tracker, and also to investigate the BER performance of the receiver. As already mentioned, channel filtering is carried out numerically with an oversampling factor of $4 \div 8$ times the bit rate, while reconstruction of the training signal is carried out on T_b-spaced samples.

The results presented in the following were derived under the assumption that each residual frequency offset estimate $\Delta\hat{f}_{k-1}$ is generated from the observation of $L = 10$ consecutive

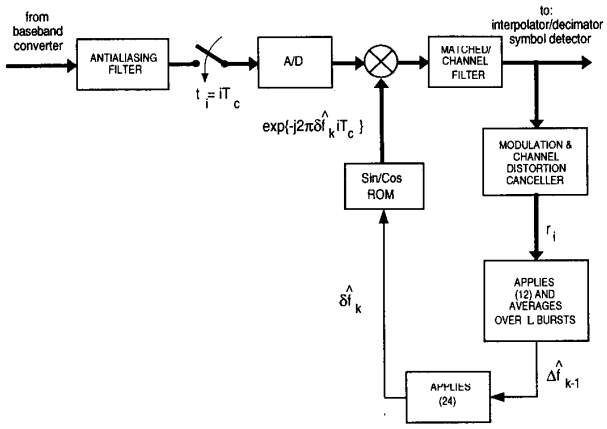

Fig. 12 - Functional block diagram of the receiver employing a closed loop frequency tracker

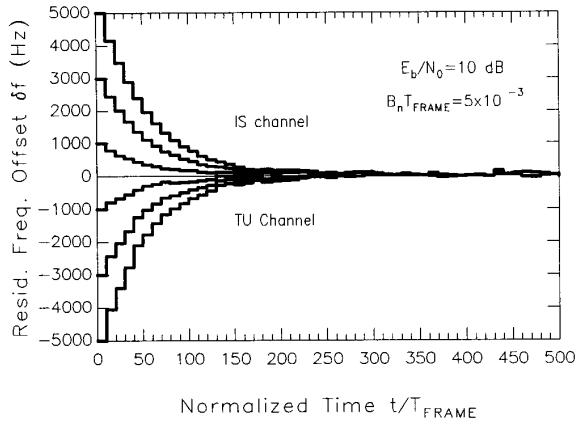

Fig. 13 - Frequency acquisition transients in the GSM receiver (IS and TU channels)

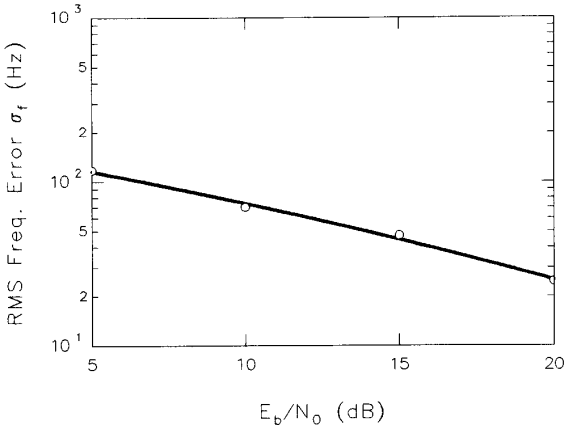

Fig. 14 - RMS frequency jitter of the GSM receiver (TU channel)

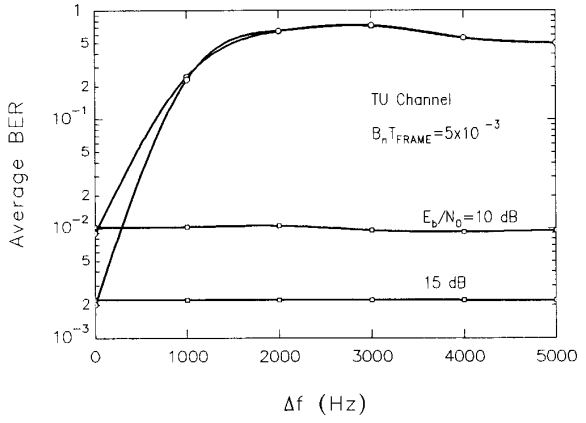

Fig. 15 - Average BER vs. Δf for the GSM receiver on the TU channel.

bursts, i. e., $\delta\hat{f}_k$ is updated every $T_\Delta = 10T_{FRAME} \simeq 46.2$ ms. Also, the stepsize γ is such that the normalized loop noise equivalent bandwidth is fixed at $B_nT_{FRAME} = 5 \cdot 10^{-3}$. When dealing with the standard GSM channels, we conventionally use the symbol E_b to denote the average bit energy received through the 0-dB path.

Figure 13 shows some examples of frequency acquisition of the GSM receiver of Fig. 12. The curves were obtained by simulation letting E_b/N_0 = 10 dB and starting the acquisition from various normalized frequency offsets ΔfT_b. The curves above the horizontal axis (positive frequency offsets) were derived for the IS propagation channel, while those characterized by negative initial offsets are relevant to a TU channel. The acquisition times are essentially the same with these two channels, and the error fluctuations around the steady-state value, although a little more pronounced for the TU channel, are still moderate and compatible with a correct operation of the receiver. Slightly better results were obtained with the RA and HT channels.

Figure 14 shows a plot of the RMS value σ_f of the closed-loop frequency estimation error vs. E_b/N_0 on the TU channel, comparing simulations (marks) and analytical results (solid curve). These latter were derived under the assumption, validated by simulation, of a flat power spectral density of the loop error signal $\Delta\hat{f}_{k-1}$.

A few words on the impact of the frequency recovery loop on the average BER of the receiver are now in order. Data symbol recovery is accomplished in the GSM receiver by means of a maximum likelihood sequence estimation strategy (in the form of a so-called Viterbi equalizer), to compensate for channel distortions [12]. Some results are summarized in Fig. 15, where the average BER of such a receiver, derived by simulation, is plotted as a function of Δf for the TU channel when E_b/N_0 equals 10 dB or 20 dB. Squares and dots indicate presence and absence of the frequency recovery loop,

respectively, and solid curves are used to interpolate the simulation results. It is seen that the frequency recovery loop makes the receiver almost insensitive to the frequency offset, setting its performance at approximately the same level as in the ideal case, i. e., when $\Delta f = 0$ and the loop is absent.

APPENDIX

We compute hereafter an expression for the error variance $E\{(\Delta\hat{f} - \Delta f)^2\}$ of estimator (12) under the assumptions $\rho \gg 1$ and $2\pi\Delta f T_s M \ll 1$ (asymptotic error variance). To simplify notations let

$$\xi \triangleq \exp[j\pi\Delta f T_s(M+1)] \tag{A1}$$

$$\hat{\xi} \triangleq \exp[j\pi\Delta\hat{f}T_s(M+1)] = \sum_{m=1}^{M} R(m) = \sum_{m=1}^{M} \frac{1}{N-m} \sum_{k=m+1}^{N} r_k r_{k-m}^*$$

(see (12)) (A2)

$$\varepsilon \triangleq \pi(\Delta\hat{f} - \Delta f)T_s(M+1) \tag{A3}$$

so that

$$E\{(\Delta\hat{f} - \Delta f)^2\} = \frac{1}{\pi^2 T_s^2 (M+1)^2} E\{\varepsilon^2\}. \tag{A4}$$

On the other hand,

$$\varepsilon = \arg\left\{\hat{\xi}\xi^*\right\} = \arg\left\{\sum_{m=1}^{M} \frac{1}{N-m} \sum_{k=m+1}^{N} r_k r_{k-m}^* \xi^*\right\}. \tag{A5}$$

Recalling (1) and letting $\varpi \triangleq \pi\Delta f T_s$, we get

$$\varepsilon = \arg\left\{ \sum_{m=1}^{M} \frac{1}{N-m} \sum_{k=m+1}^{N} \left[e^{j2\pi m} + e^{j2\pi k}\tilde{v}_{k-m}^* + e^{-j2\pi(k-m)}\tilde{v}_k + \tilde{v}_k\tilde{v}_{k-m}^*\right] e^{-j\pi(M+1)} \right\}. \tag{A6}$$

Under the assumption of high CNR, the noise×noise term $\tilde{v}_k\tilde{v}_{k-m}^*$ can be neglected, yielding

$$\varepsilon \cong \arg\left\{1 + \frac{\sin\varpi}{\sin(M\varpi)} \cdot \sum_{m=1}^{M} \frac{1}{N-m} \sum_{k=m+1}^{N} \left[e^{j\pi(2k-M-1)}\tilde{v}_{k-m}^* + e^{-j\pi(2k-2m+M+1)}\tilde{v}_k\right]\right\}$$

$$\cong \mathrm{Im}\left\{\frac{\sin\varpi}{\sin(M\varpi)} \cdot \sum_{m=1}^{M} \frac{1}{N-m} \sum_{k=m+1}^{N} \left[e^{j\pi(2k-M-1)}\tilde{v}_{k-m}^* + e^{-j\pi(2k-2m+M+1)}\tilde{v}_k\right]\right\} \tag{A7}$$

After squaring (A7) and taking the expectation, we are left with

$$E\{\varepsilon^2\} \cong \frac{\sigma^2}{2} \frac{\sin^2\varpi}{\sin^2(\varpi M)} \sum_{m=1}^{M}\sum_{r=1}^{M} \frac{1}{(N-m)(N-r)} \cdot \sum_{k=m+1}^{N}\sum_{l=r+1}^{N} \{-2\cos[2\varpi(k+r-l-M-1)]\delta(l-k+m) + 2\cos[2\varpi(k-l)]\delta(k-m-l-r) - 2\cos[2\varpi(m-k+l-M-1)]\delta(k-l-r) + 2\cos[2\varpi(k-m+r-l)]\delta(l-k)\} \tag{A8}$$

so that, after rather tedious but straightforward manipulations, we find

$$E\{(\Delta\hat{f} - \Delta f)^2\}\Big|_{\rho\to\infty} \cong \frac{1}{\pi^2 T_s^2 (M+1)^2 \rho} \frac{\sin^2(\pi\Delta f T_s)}{\sin^2(\pi\Delta f T_s M)} \cdot \sum_{m=1}^{M}\sum_{r=1}^{M} \left\{\frac{\min(N-r, N-m)}{(N-r)(N-m)} \cos[2\pi\Delta f T_s(m-r)] - \frac{(N-r-m)\,\mathrm{u}(N-r-m)}{(N-r)(N-m)} \cos[2\pi\Delta f T_s(m+r-M-1)]\right\} \tag{A9}$$

where $\mathrm{u}(\cdot)$ denotes the unit step function.

Equation (A9) shows a dependence of the AEV on the frequency offset Δf. On the other hand, when $2\pi\Delta f T_s M \ll 1$ the following approximate relation holds true

$$[\sin(\pi\Delta f T_s)/\sin(\pi\Delta f T_s M)]^2 \cong 1/M^2 \tag{A10}$$

and the cosine functions can be replaced by unity. As a final result, we are led to

$$E\{(\Delta\hat{f} - \Delta f)^2\}\Big|_{\rho\to\infty} \cong \frac{1}{\pi^2 T_s^2 (M+1)^2 \rho} \frac{1}{M^2} \cdot \sum_{m=1}^{M}\sum_{r=1}^{M} \left\{\frac{\min(N-r, N-m)}{(N-r)(M-m)} - \frac{(N-r-m)\,\mathrm{u}(N-r-m)}{(N-r)(M-m)}\right\} \tag{A11}$$

REFERENCES

[1] V. K. Bhargava, D. Haccoun, R. Matyas and P. P. Nuspl, *Digital Communications by Satellite*. New York: John Wiley & Sons, 1981.

[2] D. J. Goodman, "Trends in Cellular and Cordless Communications," *IEEE Commun. Magazine*, vol. 29, pp. 31-40, June 1991.

[3] C. Heegard, J. A. Heller and A. J. Viterbi, "A Microprocessor-Based PSK Modem for Packet Transmission over Satellite Channels," *IEEE Trans. Commun.*, vol. COM-26, pp. 552-564, May 1978.

[4] M. K. Simon and D. Divsalar, "Doppler-Corrected Differential Detection of MPSK," *IEEE Trans. Commun.*, vol. COM-37, pp. 99-109, Feb. 1989.

[5] J. C.-I. Chuang and N. R. Sollenberger, "Burst Coherent Demodulation with Combined Symbol Timing, Frequency Offset Estimation, and Diversity Selection," *IEEE Trans. Commun.*, vol. COM-39, pp. 1157-1164, July 1991.

[6] S. Tretter, "Estimating the Frequency of a Noisy Sinusoid by Linear Regression," *IEEE Trans. Inform. Theory*, vol. IT-31, pp. 832-835, Nov. 1985.

[7] S. Bellini, C. Molinari and G. Tartara, "Digital Frequency Estimation in Burst Mode QPSK Transmission," *IEEE Trans. Commun.*, Vol. 38, pp. 959-961, July 1990.

[8] GSM Recommendation 11.10, Part II.3, V. 1.07.00, March 1990.

[9] M. P. Fitz, "Planar Filtered Techniques for Burst Mode Carrier Synchronization," *IEEE GLOBECOM '91*, Phoenix, AZ, Dec. 1991, paper 12.1.

[10] H. L. Van Trees, *Detection, Estimation and Modulation Theory*, vol. I-II. New York: John Wiley & Sons, 1968.

[11] N. A. D'Andrea, U. Mengali and R. Reggiannini, "The Modified

Cramér-Rao Bound and Its Application to Synchronization Problems," *IEEE Trans. Commun.*, vol. COM-42, pp. 1391-1399, Feb./March/April 1994.

[12] C. Lombardi, M. Luise and R. Reggiannini, "Performance Analysis of an Adaptive Receiver Structure for Digital Mobile Communications," *Int. Journal of Digital and Analog Commun. Systems*, vol. 4, pp. 11-20, J. Wiley & Sons, 1991.

[13] M. Luise and U. Mengali, "A New Interpretation of the Average Matched Filter for MSK-Type Receivers," *IEEE Trans. Commun.*, vol. COM-39, pp. 14-16, Jan. 1990.

[14] D. C. Rife and R. R. Boorstyn, "Single Tone Parameter Estimation from Discrete-Time Observations," *IEEE Trans. Inform. Theory*, vol. IT-20, pp. 591-598, Sept. 1974.

[15] S. A. Kay, *Modern Spectral Estimation*. Englewood Cliffs: Prentice-Hall Signal Processing Series, Oppenheim ed., 1988.

[16] ———, "A Fast and Accurate Single Frequency Estimator," *IEEE Trans. Acoust. Speech Sig. Proc.*, vol. ASSP-37, pp. 1987-1990, Dec. 1989.

[17] F. M. Gardner, "A BPSK/QPSK Timing-Error Detector for Sampled Receivers," *IEEE Trans. Commun.*, vol. COM-34, pp. 423-429, May 1986.

[18] GSM Recommendation 05.05, *Radio Transmission and Reception*, V. 3.11.0, ETSI/PT 12, Jan. 1990.

[19] H. Meyr and G. Ascheid, *Synchronization in Digital Communications*. New York: John Wiley & Sons, 1990.

Marco Luise (M'88) was born in Livorno, Italy, in 1960. He received the Doctor Engineer (cum Laude) and Research Doctor degrees in Electronic Engineering from the University of Pisa, Italy, in 1984 and 1989, respectively. In 1987 he spent one year at the European Space Research and Technology Centre (ESTEC), Noordwijk, The Netherlands, as a Research Fellow of the European Space Agency (ESA). Since 1988 to 1991 he was a Research Scientist of CNR, the Italian National Research Council, at the Centro Studio Metodi Dispositivi Radiotrasmissioni (CSMDR), Pisa. In 1991 and 1993 he chaired the 5th and 6th editions of the Tirrenia International Workshop on Digital Communications, respectively. He is now holding the position of Associate Professor at the Department of Information Engineering of the University of Pisa. Prof. Luise's main research interests lie in the broad area of communication theory, with particular emphasis on mobile and satellite communication systems and spread-spectrum communications.

Ruggero Reggiannini received the Dr. Ing. degree in Electronic Engineering from the University of Pisa, Italy, in 1978.

From 1978 to 1983 he was with USEA S.p.A., where he was engaged in the design and development of underwater acoustic systems. Since 1984 he has been with the Department of Information Engineering of the University of Pisa, where he is currently Associate Professor of Radio Communications. His research interests are in the field of digital satellite and mobile communication systems.